Study of neutrino oscillations with the atmospheric neutrino data from Super-Kamiokande

Takaaki Kajita [a*] (For the Super-Kamiokande collaboration)

[a]Research Center for Cosmic Neutrinos, Institute for Cosmic Ray Research, Univ. of Tokyo
5-1-5 Kashiwa-no-ha, Kashiwa, Chiba 277-8582, Japan

Recent data from Super-Kamiokande on atmospheric neutrinos are presented. The atmospheric neutrino data give accurate information on neutrino mass and mixing. The data are explained by two flavor $\nu_\mu \to \nu_\tau$ oscillations with $\Delta m^2 = (1.5-5) \times 10^{-3}\mathrm{eV}^2$ and $\sin^2 2\theta > 0.88$. An alternative explanation, $\nu_\mu \to \nu_{sterile}$ oscillations, is disfavored at 99% C.L. by a detailed analysis of NC enriched and high energy atmospheric neutrino events.

1. Introduction

Atmospheric neutrino data have been contributing to studies of neutrino oscillations. The measured values of the (μ/e) ratio of atmospheric neutrino events (which is closely related to the (ν_μ/ν_e) flux ratio) by Kamiokande were significantly smaller than the Monte Carlo (MC) predictions [1] [2]. The uncertainty in the absolute flux prediction is about 20%. However, the (ν_μ/ν_e) flux ratio is predicted with an accuracy of better than 5% over a wide energy range. Also a zenith-angle dependent deficit of μ-like events was observed by Kamiokande [2] at high energies. The up/down ratio of the flux is calculated to an accuracy of better than a few % and is approximately unity above a few GeV neutrino energies. These observations strongly suggested neutrino oscillations. In 1998, Super-Kamiokande reported that the atmospheric neutrino data gave evidence for neutrino oscillations [3].

Super-Kamiokande is a 50 kton water Cherenkov detector. The detector is consisted of two parts, an inner detector and an outer detector. The pulse height and timing information recorded by the inner detector photomultiplier tubes are used to reconstruct kinematics of neutrino events. The outer detector, which surrounds the inner detector completely, is useful to identify incoming cosmic ray muons and exiting particles in neutrino events which occurred in the inner detector. The fiducial volume for various physics analyses is 22.5 kton. In this article, we present the atmospheric neutrino data from Super-Kamiokande based on three years of the detector exposure.

2. Atmospheric neutrino data

Super-Kamiokande has observed 9178 fully-contained (FC) and 665 partially-contained (PC) events during a 70 kton·yr exposure. For the analysis of FC events, only single-ring events were used. Single-ring events were identified as e-like or μ-like. The threshold momentum for the analysis were 100 and 200 MeV/c for e-like and μ-like events, respectively. The FC events were separated into "sub-GeV" ($E_{vis} < 1330$ MeV) and "multi-GeV" ($E_{vis} > 1330$ MeV) samples, where E_{vis} was defined to be the energy of an electron that would produce the observed amount of Cherenkov light. In a full MC simulation, 87% (95%) of sub-GeV e-like (μ-like) events were ν_e (ν_μ) charged-current (CC) interactions and 84% (99%) of multi-GeV e-like (μ-like) events were ν_e (ν_μ) CC interactions. PC events were estimated to be 97% ν_μ CC interactions; hence, all PC events were classified as μ-like.

Table 1 summarizes the atmospheric neutrino data and the $(\mu/e)_{data}/(\mu/e)_{MC}$ measurements from Super-Kamiokande. The observed ratios

*This work was partly supported by the Japanese Ministry of Education, Science, Sports and Culture.

Table 1
Summary of the atmospheric neutrino data from Super-Kamiokande (70 kton·yr). In the Monte Carlo simulation, the atmospheric neutrino flux [4] without neutrino oscillations is used.

	Data	MC
Sub-GeV FC		
e-like	2531	2402.6
μ-like	2486	3620.9
multi-ring	1885	2321.5
$(\mu/e)_{data}/(\mu/e)_{MC}$ =0.65±0.02±0.05		
Multi-GeV FC		
e-like	576	555.4
μ-like	502	738.7
multi-ring	1198	1470.1
PC (= μ-like)	665	945.1
$(\mu/e)_{data}/(\mu/e)_{MC} = 0.67^{+0.04}_{-0.03} \pm 0.08$		

were significantly smaller than unity.

The zenith angle distributions for the FC and PC events are shown in Figure 1. The μ-like data, especially multi-GeV μ-like data, exhibited a strong up-down asymmetry in zenith angle while no significant asymmetry was observed in the e-like data. At low energies, below ~400 MeV/c, the lepton direction has little correlation with the neutrino direction. Therefore, the zenith angle dependence of the flux as a consequence of neutrino oscillations is largely washed out below 400 MeV/c lepton momentum. The correlation angle becomes smaller with increasing lepton momentum. We define the up-down double-ratio, $(U/D)_{Data}/(U/D)_{MC}$, where U is the number of upward-going events ($-1 < \cos\Theta < -0.2$) and D is the number of downward-going events ($0.2 < \cos\Theta < 1$). This ratio is expected to be consistent with unity within errors for no neutrino oscillations. The $(U/D)_{Data}/(U/D)_{MC}$ value for the multi-GeV FC+PC μ-like events, $0.52 \pm 0.04(stat.) \pm 0.01(syst.)$, deviated from unity by 9 standard deviations. This result, which is close to 0.5, suggests a near-maximal neutrino mixing, since $(U/D)_{Data}/(U/D)_{MC} \simeq 1-(\sin^2 2\theta)/2$ to first approximation, assuming that there is no (full) oscillation effect for downward-(upward-)going particles, and averaging over the energy spectrum.

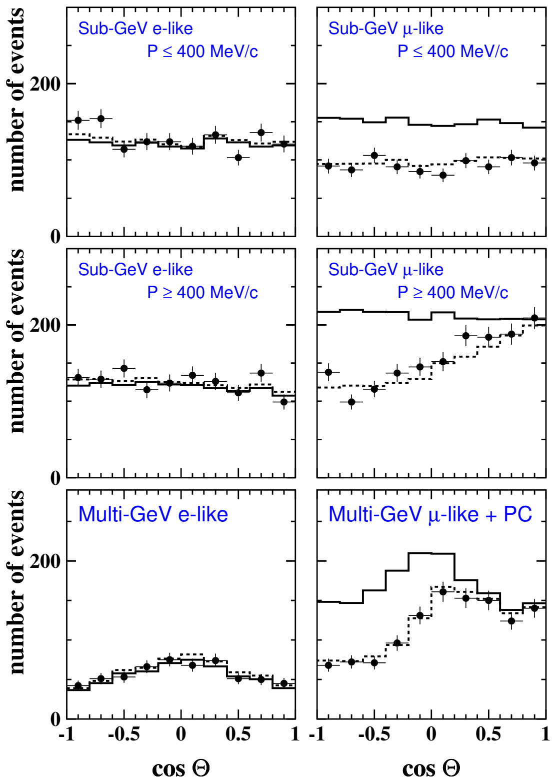

Figure 1. Zenith-angle distributions for (left) e-like and (right) μ-like events. The top figures show those with momentum lower than 400 MeV/c, the middle ones for sub-GeV events with momentum higher than 400 MeV/c, and the bottom ones for multi-GeV events. CosΘ =1 means down-going particles. The solid histograms show the MC prediction without neutrino oscillations. The dashed histograms show the MC prediction for $\nu_\mu \to \nu_\tau$ oscillations with $\sin^2 2\theta$ =1 and Δm^2 =3.2×10^{-3} eV^2. In the oscillation histograms, the absolute normalization was adjusted to get the minimum χ^2.

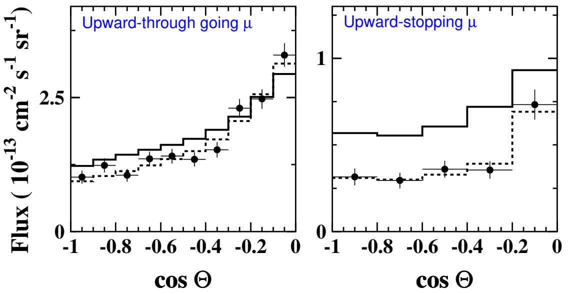

Figure 2. Zenith-angle distributions for upward-going muon fluxes. Circles with error bars show the upward through-going(left) and stopping(right) muon data. Error bars show statistical + experimental systematic errors. Estimated background events are subtracted. The solid histograms show the expected fluxes for the null oscillation case. The dashed histograms show the expected fluxes for the $\nu_\mu \to \nu_\tau$ oscillation case with $\sin^2 2\theta$ =1.0 and $\Delta m^2 = 3.2 \times 10^{-3}$ eV^2.

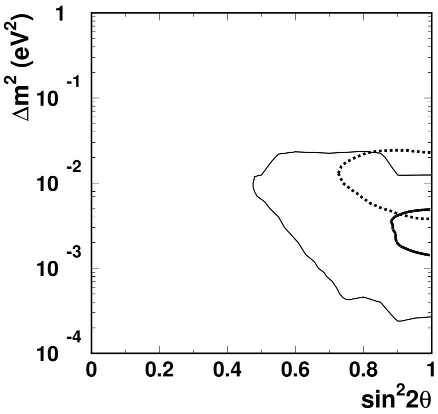

Figure 3. 90% C.L. allowed parameter region for $\nu_\mu \to \nu_\tau$ oscillations by a combined analysis of FC, PC, upward stopping muon and upward through-going muon events from Super-Kamiokande (thick line). Results from Kamiokande [6] (FC + PC + upward-going muons, thick dashed line) and Soudan-2 [7] (FC events, thin line) are also shown.

In addition to the contained events, Super-Kamiokande has observed 1269 upward through-going muon events (including 9.1±0.8 estimated background events) during 1138 detector live days [5]. 311 upward stopping muon events (including 21.4±8.8 estimated background events) have also been observed during 1117 detector live days [5]. Figure 2 shows the zenith-angle distributions of the upward going muon fluxes. The background events are expected to be in the most horizontal bins and are subtracted. The prediction for the through-going muons had a flatter zenith-angle distribution than the data. The observed flux of upward stopping muons was approximately a factor of two smaller than the prediction. These data are explained by neutrino oscillations.

2.1. 2 and 3 flavor oscillation analyses

Since the contained events and upward-going muon events consistently suggested neutrino oscillations, an allowed region of the neutrino oscillation parameters assuming pure $\nu_\mu \to \nu_\tau$ oscillations was obtained using all the atmospheric neutrino data from Super-Kamiokande. In the oscillation analysis, various systematic errors were taken into account. They (and their size) are; absolute normalization (25%, but this was fitted as a free parameter), sub-GeV $(\mu/e)_{data}/(\mu/e)_{MC}$ (8%), multi-GeV $(\mu/e)_{data}/(\mu/e)_{MC}$ (12%), normalization of PC events relative to FC events (8%), normalization of upward stopping muons relative to FC+PC events (7%), normalization of upward through-going muons relative to upward-stopping muons (7%), energy spectrum index of neutrinos (0.05), sub-GeV up-down ratio (2.4%), multi-GeV up-down ratio (2.7%), vertical-horizontal ratio for FC+PC (4%) vertical-horizontal ratio for upward going muons (3%) and L/E (15%). The allowed region is shown in Figure 3. The best fit point was found at ($\sin^2 2\theta$, Δm^2) = (1.0, 3.2×10^{-3}eV^2). Even if the analysis was extended to the unphysical region of $\sin^2 2\theta$ >1, the best fit point was the same. The 90% C.L. allowed region of the oscillation parameters was; $1.5 \times 10^{-3} < \Delta m^2 < 5 \times 10^{-3}$eV^2 and $\sin^2 2\theta$ >0.88.

There is now intense flux calculation activity in which the fluxes are calculated based on a full three dimensional simulation of the particle trajectory and the Earth [8] [9]. As the full three-dimensional calculations predict an enhancement of horizontal fluxes in the sub-GeV energy region, we have estimated the oscillation parame-

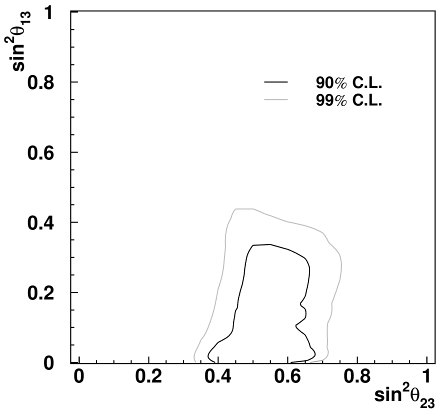

Figure 4. Allowed region on the $\sin^2\theta_{13}$ and $\sin^2\theta_{23}$ plane obtained by a 3 flavor analysis of the FC+PC data. Black and gray lines show 90 and 99%C.L. allowed regions, respectively.

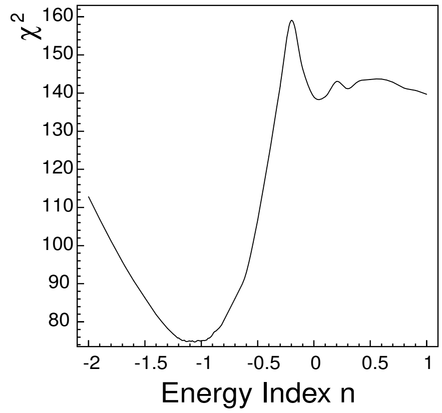

Figure 5. χ^2 values of the fit to the atmospheric neutrino data as a function of the energy index n and unconstrained oscillation factors α and β. The χ^2 value is calculated assuming an oscillation probability $P(\nu_\mu \to \nu_\mu) = 1 - \sin^2\alpha \cdot \sin^2(\beta \cdot L \cdot E^n)$.

ters based on fluxes by a three-dimensional calculation [9]. In spite of the horizontal enhancement of the flux, the predicted zenith-angle distributions of μ-like and e-like events are similar due to a large neutrino-lepton scattering angle in the sub-GeV energy region. Therefore, the allowed parameter region based on one-dimensional and three-dimensional fluxes turned out to be similar (preliminary). (It is still possible that fluxes based on three-dimensional calculations could suggest slightly higher Δm^2 value than the one-dimensional fluxes do.) In any case, we need more studies for the three-dimensional flux calculation effects.

Super-Kamiokande has also carried out a 3 flavor neutrino oscillation analysis. It was assumed that the mass difference between the lightest and the second lightest neutrinos is very small and therefore the effect of the oscillation between these two neutrino eigenstates is invisible in atmospheric neutrinos. The allowed region was obtained on a three-dimensional space of $\sin^2\theta_{13}$, $\sin^2\theta_{23}$ and $\Delta m^2 (\equiv \Delta m^2_{13} = \Delta m^2_{23})$. An allowed region on the $\sin^2\theta_{13}$ and $\sin^2\theta_{23}$ plane is shown in Figure 4. (Note that the axes are $\sin^2\theta_{ij}$, not $\sin^2 2\theta_{ij}$.) No evidence for non-zero $\sin^2\theta_{13}$ has been found. This result is consistent with the CHOOZ [10] and Palo Verde [11] results. We comment that the constraint from the CHOOZ experiment [10] on $\sin^2\theta_{13}$ in the Δm^2 range between 1.5 and 5 $\times 10^{-3}$eV^2 is much stronger than that from Super-Kamiokande.

2.2. Energy dependence of oscillations

Super-Kamiokande has studied the energy dependence of the neutrino oscillations. For this purpose, the atmospheric neutrino data (including upward going muons) were fitted with a form of $P(\nu_\mu \to \nu_\mu) = 1 - \sin^2\alpha \cdot \sin^2(\beta \cdot L \cdot E^n)$, where α, β and n were fitted parameters [12]. Figure 5 shows the n dependence of the χ^2 value of the fit. The energy dependence expected by the standard neutrino oscillation generated by neutrino mass and mixing ($n = -1$) was favored by the data (the fitted value of n was -1.06 ± 0.14), and models that predict other energy dependence of the oscillations were strongly disfavored.

2.3. $\nu_\mu \to \nu_\tau$ versus $\nu_\mu \to \nu_{sterile}$ oscillations

According to a neutrino oscillation analysis using FC events, both $\nu_\mu \to \nu_\tau$ and $\nu_\mu \to \nu_{sterile}$ were almost equally allowed. $\nu_{sterile}$ is a hypothetical neutrino-like particle which does not interact with matter by either CC or NC weak interactions. Since the existence of $\nu_{sterile}$ has significant impact on particle physics and cosmology, it must be studied seriously whether $\nu_\mu \to \nu_{sterile}$ oscillations are really favored by the atmospheric

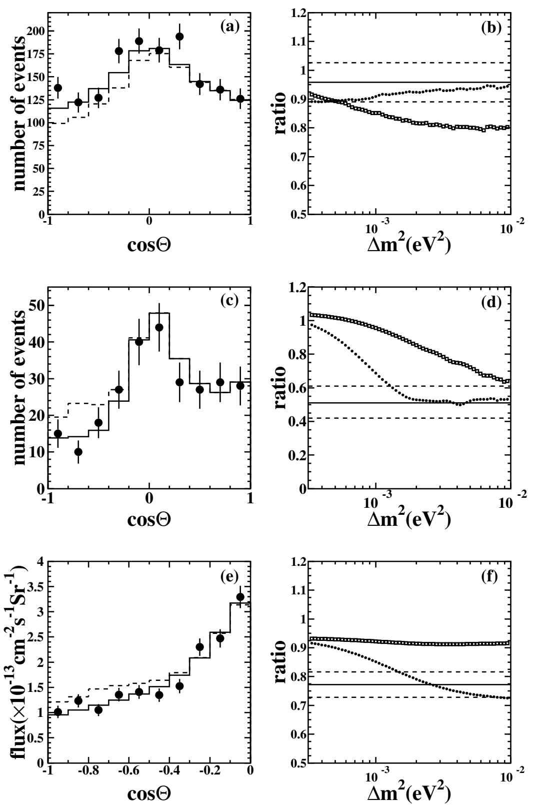

Figure 6. Zenith-angle distributions for: (a)multi-ring events with the most energetic ring being e-like and E_{vis} >400 MeV, (c)PC events with E_{vis} >5 GeV, and (e)upward through-going muon events. In (a), (c) and (e), solid (dashed) histograms show predictions for $\nu_\mu \to \nu_\tau$ ($\nu_\mu \to \nu_{sterile}$) oscillations with $\Delta m^2 = 3 \times 10^{-3} eV^2$ and $\sin^2 2\theta = 1.0$. The predictions are normalized so that the number of observed and predicted events are equal at $0.4 < cos\Theta < 1.0$ for (a) and (c) and at $-0.4 < cos\Theta < 0.0$ for (e). In (b) and (d), expected $Up(-1 < cos\Theta < -0.4)/Down(0.4 < cos\Theta < 1)$ ratios of the corresponding data sets are plotted as a function of Δm^2. In (f), expected $Vertical(-1 < cos\Theta < -0.4)/Horizontal(-0.4 < cos\Theta < 0)$ ratios for the upward through-going muon events are plotted. In these figures, dots are for $\nu_\mu \to \nu_\tau$ and empty squares are for $\nu_\mu \to \nu_{sterile}$ with $\sin^2 2\theta$ =1. Also shown in the same figures are the ratios for the data. The solid lines show the central values for the data and the dashed lines show the $\pm 1\sigma$ statistical errors.

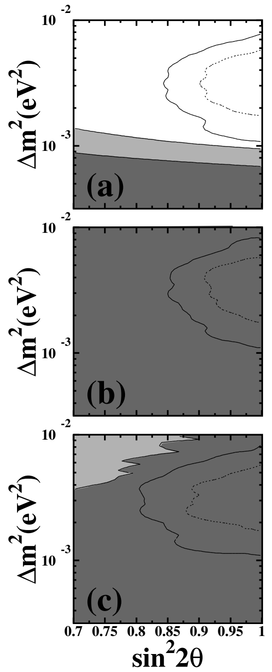

Figure 7. 90 and 99% C.L. allowed regions of neutrino oscillation parameters obtained by the FC events are shown by thin dotted and solid lines, respectively, for (a) $\nu_\mu \to \nu_\tau$, (b) $\nu_\mu \to \nu_{sterile}$ (Δm^2 >0), and (c) $\nu_\mu \to \nu_{sterile}$ (Δm^2 <0). Also shown are excluded regions from a combined analysis of the multi-ring, high-energy-PC and upward through-going muon events. Light-grey and dark-grey regions show the 90% and 99% C.L. exclusion regions, respectively.

neutrino data.

There are several ways to discriminate between the two possibilities. One possibility is to use a matter effect for upward going neutrino events [13] [14]. In the case of $\nu_\mu \to \nu_\tau$ oscillations, the matter effect does not change the oscillation probability. On the other hand, in the case of $\nu_\mu \to \nu_{sterile}$ oscillations, the matter effect might change the oscillation probability significantly. For $\Delta m^2 \sim 3 \times 10^{-3}$eV^2, the oscillation probability is expected to be significantly different only for high energy (> 20 GeV) atmospheric neutrinos traveling through the Earth. In addition, the zenith angle distribution of a NC enriched sample is useful to discriminate between the two possibilities, because the NC events should be affected only for $\nu_\mu \to \nu_{sterile}$ oscillations.

An analysis using multi-ring, high-energy PC with E_{vis} >5 GeV, and upward through-going muon events was carried out [15]. Multi-ring events with the most energetic ring being e-like and E_{vis} >400 MeV were used. The estimated fraction of NC events (in the absence of neutrino oscillations) was 29%. Figures 6 (a), (c) and (e) show the zenith angle distributions for these events, together with neutrino oscillation predictions. In all three samples, the differences between the two hypotheses are significant for upward-going directions. Since the shape of the zenith angle distributions is predicted accurately [16], we studied the $Up/Down$ or $Vertical/Horizontal$ ratio depending on the data sample, as shown in Figures 6 (b), (d) and (f). The systematic errors in these ratios were estimated to be $(3-4)$% depending on the data sample [15]. In these three samples, the data disfavored $\nu_\mu \to \nu_{sterile}$ oscillations.

Finally, the two oscillation hypotheses were tested by combining these three studies by a χ^2 method:

$$\chi^2 = \chi^2_{multi-ring} + \chi^2_{PC} + \chi^2_{upgoing-muon}.$$

If the χ^2 value is larger than 6.3 (11.3), the hypothesis is disfavored at 90 (99)% C.L.. Figure 7 shows the results of this hypothesis test. Because the matter effect and therefore the oscillation probability depends on $(m_j^2 - m_i^2)$ rather than $|m_j^2 - m_i^2|$ for $\nu_\mu \to \nu_{sterile}$ oscillations, both positive and negative $\Delta m^2 (\equiv m_j^2 - m_i^2)$ were tested. The $\nu_\mu \to \nu_\tau$ oscillation hypothesis did not contradict the data in this analysis. On the other hand, the parameter regions suggested by the analysis of FC events for the pure $\nu_\mu \to \nu_{sterile}$ hypothesis were disfavored at 99% C.L..

3. Summary

Both the zenith angle distribution for μ-like events and the (μ/e) values were significantly different from the predictions in the absence of neutrino oscillations. The data were in good agreement with $\nu_\mu \to \nu_\tau$ oscillations. This conclusion was supported by the upward-going muon data. By using all the atmospheric neutrino data from Super-Kamiokande, the 90% C.L. allowed region on $\nu_\mu \to \nu_\tau$ oscillation parameters was: $1.5 \times 10^{-3} < \Delta m^2 < 5 \times 10^{-3}$eV^2 and $\sin^2 2\theta$ >0.88. The matter effect and the neutral current events have been used to discriminate between $\nu_\mu \to \nu_\tau$ and $\nu_\mu \to \nu_{sterile}$ oscillations. The data disfavored the pure $\nu_\mu \to \nu_{sterile}$ oscillation hypothesis at 99% C.L..

REFERENCES

1. K. S. Hirata *et al.*, Phys. Lett. B **205** (1988) 416; Phys. Lett. B **280** (1992) 146.
2. Y. Fukuda *et al.*, Phys. Lett. B **335** (1994) 237.
3. Y. Fukuda *et al.*, Phys. Lett. B **433** (1998) 9; Phys. Lett. B **436** (1998) 33; Phys. Rev. Lett. **81** (1998) 1562.
4. M. Honda *et al.*, Phys. Rev. D **52** (1995) 4985.
5. Y. Fukuda *et al.*, Phys. Rev. Lett. **82** (1999) 2644; Phys. Lett. B **467** (1999) 185.
6. S. Hatakeyama *et al.*, Phys. Rev. Lett. **81** (1998) 2016.
7. W. W. M. Allison *et al.*, Phys. Lett. B **449** (1999) 137; W. A. Mann, hep-ex/0007031.
8. G. Battistoni *et al.*, Astropart. Phys. **12**, (2000) 315.
9. P. Lipari, Astropart. Phys. **14**, (2000) 153.
10. M. Apollonio *et al.*, Phys. Lett. B **420** (1998) 397. Phys. Lett. B **466** (1999) 415.
11. F. Boehm *et al.*, Phys. Rev. Lett. **84** (2000) 3764; Phys. Rev. D **62** (2000) 072002.
12. G. L. Fogli *et al.*, Phys. Rev. D **60** (1999) 053006.
13. Q. Y. Liu, S. P. Mikheyev, and A. Yu. Smirnov, Phys. Lett. B **440** (1998) 319.
14. P. Lipari, and M. Lusignoli, Phys. Rev. D **58**, (1998) 073005.
15. S. Fukuda *et al.*, Phys. Rev. Lett. **85** (2000) 3999.
16. P. Lipari, talk presented at the XIX International Conference on Neutrino Physics and Astrophysics, Sudbury, Canada, June 2000.